10. Impact of Emissions from the Los Angeles Port Region on San Diego Air Quality During Regional Transport Events

i. Introduction

Atmospheric aerosols regionally and globally impact climate and health. Regionally transported particles contribute significantly to $PM_{2.5}$ as observed in multiple studies (319,320). Oceangoing ships emit an estimated 1.2–1.6 million metric tons (Tg) of PM_{10} per year(321) and the 2006 California Air Resources Board emissions inventory estimates that ships emit more $PM_{2.5}$ (4.94 tons/day) than refineries and power plants combined (3.45 tons/day), representing the second highest PM mobile source in Los Angeles County behind diesel trucks (5.87 tons/day) (322). In coastal regions, models show a significant impact from the emissions of ships and residual fuel combustion on air pollution levels. Strong implications exist for human health (64,323,324), but major uncertainties exist regarding the spatial and seasonal variability of particulate pollution that need further investigation (325). Field observations have confirmed that ships produce significant amounts of soot, vanadium, nickel, and sulfate (168,326). Ships typically burn residual fuel oil, which produces higher concentrations of heavy metals and soot than distillate fuels such as gasoline and diesel (77,327,328). Additional residual fuel oil sources, such as refineries, are often located near large ports and emit metal-containing particles that are particularly harmful to human health (303,329,330). These deleterious effects can be explained by the chemistry of the emissions as well as proposed synergistic relationships between coemitted chemical species such as soot and iron or vanadium and nickel (65,105,331). Recent studies in the Los Angeles and Long Beach (LA-LB) port region have shown vanadium as having the strongest correlation to reactive oxygen species using a macrophage assay (332). These negative health effects combined with the transport of particles from residual fuel combustion make it imperative to determine their contributions to the air pollution in coastal locations along the California coast.

Regionally transported air pollution has been shown to influence the San Diego region in previous studies. Aircraft measurements have shown O_3 transport from the Los Angeles (LA) basin and SO_2 transport from offshore to San Diego (333). Particles transported from LA have also been observed in San Diego at an urban freeway location by ATOFMS (334). This paper discusses distinct episodes quantifying the impact of regional transport when the air masses originated near the vicinity of the Port of LA observed by real-time single particle mass spectrometry at the Scripps Institution of Oceanography (SIO) Pier in La Jolla, California. During these transport periods, the highest concentrations of submicron carbonaceous and transition metal particles (V, Ni, and Fe) were measured. This study examines the impact of these transported aerosols on PM concentrations in the San Diego region.

ii. Experimental

a. Scripps Institution of Oceanography of Pier 2006 Study

From August 17 to October 3, 2006, sampling was conducted at the end of the SIO Pier, three hundred meters from shore. Ambient particles were sampled through a

four meter mast, seven meters above the pier, and fifteen meters above the ocean. Different instruments sampled in parallel through insulated sampling lines into multiple instruments. A five hour period of sampling on September 28, 2006 was dominated by submicron particles from a local wildfire, as determined by the ATOFMS mass spectral signatures, and because the focus of this paper is on regional transport impacts, this period is not discussed. Particle size distributions were optically measured using an aerodynamic particle sizer spectrometer (APS 3321, TSI Inc.), which measures size distributions between 0.5-3 μm. Air mass back trajectory calculations were made using HYSPLIT 4.8 (130).

b. Real-Time Single Particle Mass Spectrometry

The aerodynamic size and chemical composition of individual particles between 0.2 and 3.0 μm were measured in real-time using an aerosol time-of-flight mass spectrometer (ATOFMS); the design and details have been described in detail elsewhere (127). Briefly, particles are introduced into the ATOFMS through a converging nozzle into a differentially pumped vacuum chamber where they are accelerated to a terminal velocity. The particles then pass through two continuous wave lasers (diode pumped Nd:YAG lasers operating at 532 nm) located 6 cm apart. The velocity of each particle is used to determine the aerodynamic size using speeds from calibration with polystyrene latex spheres of known aerodynamic size, shape, and density. The sized particles are then desorbed and ionized by irradiation from a Q-switched Nd:YAG laser (266nm, 1.2-1.4 mJ/pulse) that is triggered when the particle enters the center of the mass spectrometer ion source. Positive and negative ions from each particle are detected using a dual-polarity, reflectron time-of-flight mass spectrometer. During this study, ambient particles were dried using a silica gel diffusion drier prior to analysis with the ATOFMS to decrease particle water content and, therefore, increase negative ion signal intensities (82). The ATOFMS sized and chemically analyzed 3,502,907 particles during the study.

c. Data Analysis

Single particle size and mass spectral information were analyzed with YAADA 1.2 (www.yaada.org) a data analysis toolkit for MATLAB 6.5.1 (The MathWorks, Inc.). Particles were analyzed via two approaches: (1) searching mass spectral, aerodynamic size, and temporal features and (2) clustering mass spectra using an adaptive resonance theory based neural network algorithm (ART-2a) at a vigilance factor of 0.8 (35). ART-2a combines particles into clusters based on the intensity of ion peaks in individual mass spectra. General particle types are defined by the characteristic chemical species or possible source to simplify the naming scheme; these labels do not reflect all of the species present within a specific particle type, but reflect the most intense ion peaks. Peak identifications within this paper correspond to the most probable ions for a given *m/z* ratio.

d. Scaling ATOFMS to Mass Concentrations

ATOFMS counts were scaled to number and mass concentrations using APS size-resolved number concentrations, a method shown previously to yield quantitative mass concentrations (128). Briefly, ATOFMS counts are binned into sizes that correspond to the APS size bins (0.5-2.5 μm) and scaling factors for each hour and size bin are

determined to account for ATOFMS transmission biases and busy time. After scaling the number concentrations, density is used to convert from number to mass concentrations. The bins were summed to give the mass of particulate matter less than 1 μm (PM_1) or less than 2.5 μm ($PM_{2.5}$). Scaled ATOFMS $PM_{2.5}$ mass concentrations have been shown previously to be well correlated with standard mass measurements, including the beta attenuation monitor (BAM) and micro-orifice uniform deposit impactor (MOUDI) (128). ATOFMS scaled PM_1 concentrations have been shown to track mass concentrations (335,336). Previous work has shown that with high relative humidity (129) or liquid water content conditions (48) particle density is low; thus, a density of 1.2 $\mu g/m^3$ has been used for the scaling herein due to an average relative humidity of 93% during sampling.

iii. Results and Discussion

Figure 72 shows the PM concentrations measured over the full study, highlighting the three high concentration regional transport periods. During many of the regional events, daily PM concentration maxima were observed over several days due to diurnal changes in wind speed and direction. Details on the impacts of the regional events on PM concentrations are described below. **Table 12** lists each identified regional event with accompanying properties, discussed in detail in the following sections. The fraction of PM_1 contributing to $PM_{2.5}$ is shown per hour in **Figure 73**. During submicron events, PM_1 mass accounted for 60% of the $PM_{2.5}$ mass compared to 36% on average during non-event periods.

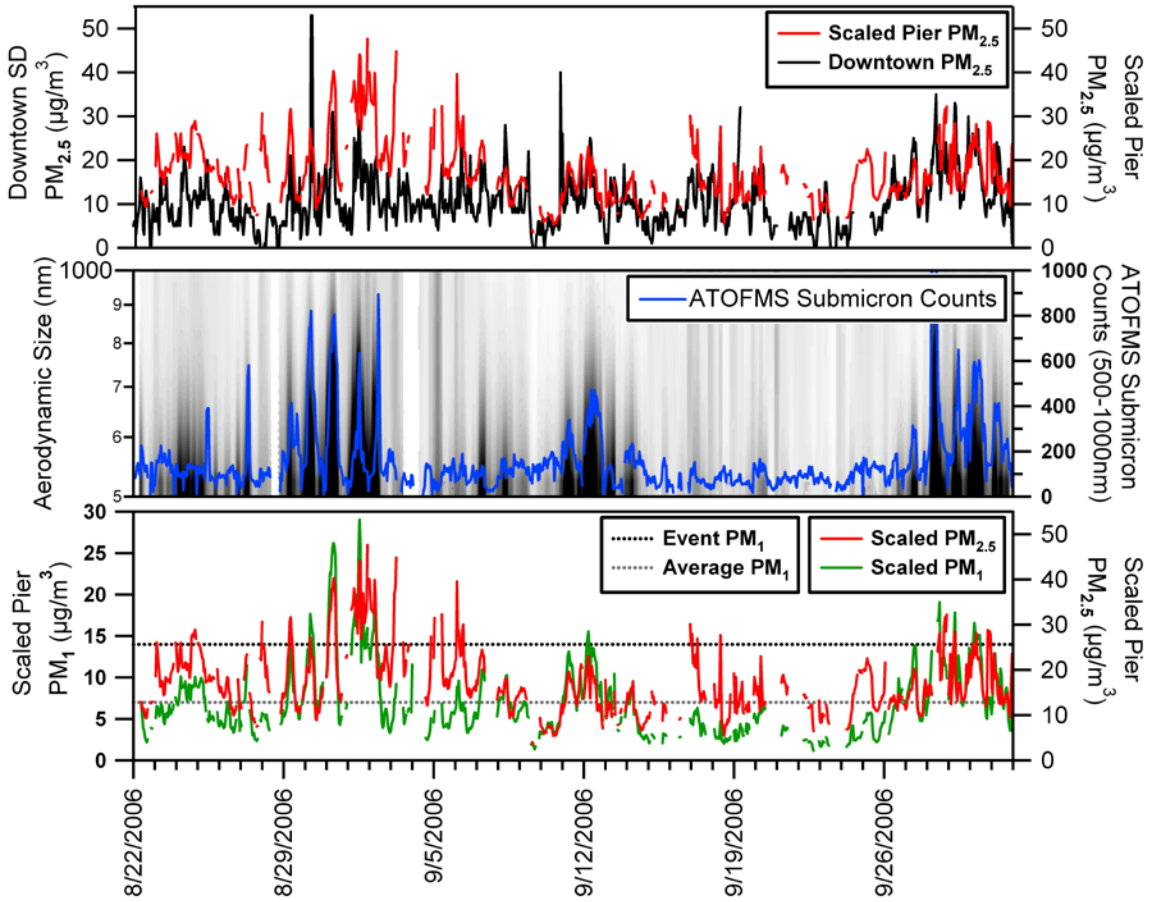

Figure 72: A) The lower portion of the graph shows time series of scaled $PM_{2.5}$ mass concentrations at the SIO Pier (red line) and $PM_{2.5}$ data from downtown San Diego (black line). B) Hourly size distributions measured by an aerodynamic particle sizer (APS) from 0.5-1 µm from August 17, 2006 – October 2, 2006. The overlaid blue line is the sum of ATOFMS counts in the 0.5-1 µm size range per hour. C) Scaled PM_1 (green line) and $PM_{2.5}$ (red line) mass concentrations are shown over the sampling period. The gray dashed line represents the average PM_1 mass concentration during the study, and the black dashed line represents the PM_1 threshold set for regional events.

Table 12: Properties of different regional events are listed including: peak PM_1 and $PM_{2.5}$ mass concentrations, fraction of PM_1 contributing to $PM_{2.5}$ mass, and the mass percentage of V-Ni-Fe and ECOC particles contributing to the PM_1 mass.

Event Number	Peak Time	Peak PM_1 ($\mu g/m^3$)	Peak $PM_{2.5}$ ($\mu g/m^3$)	$PM_1/PM_{2.5}$ Fraction	V+EC % of PM_1
1	8/29/2006 9:00	14	32	0.43	0.68
	8/30/2006 7:00	18	27	0.65	0.63
	8/31/2006 9:00	26	40	0.65	0.86
	9/1/2006 13:00	29	44	0.66	0.85
	9/2/2006 10:00	21	40	0.54	0.72
2	9/12/2006 12:00	16	23	0.67	0.72
3	9/27/2006 8:00	14	18	0.78	0.67
	9/28/2006 8:00*	21	28	0.75	0.07
	9/29/2006 11:00	18	25	0.72	0.24
	9/30/2006 5:00	17	25	0.66	0.45

* period impacted by significantly by a local fire

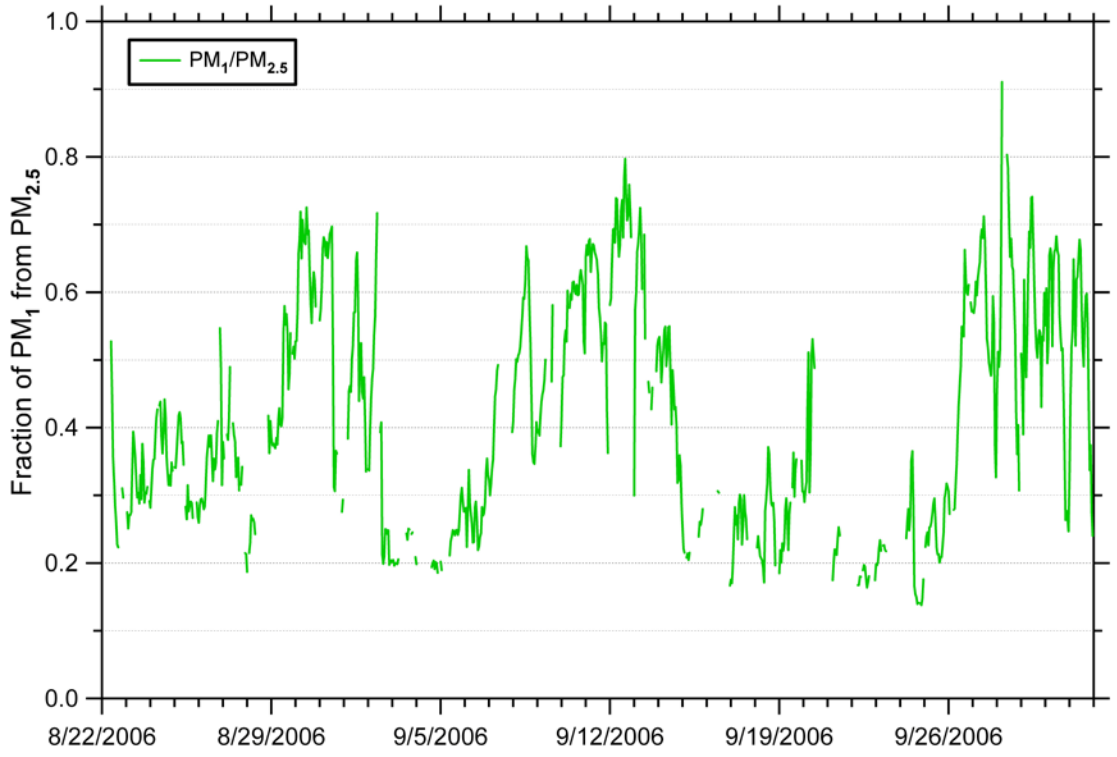

Figure 73: Fraction of scaled $PM_{2.5}$ corresponding to PM_1 hourly.

a. Mass Concentrations Across San Diego County

To verify that the scaled PM values at the SIO Pier were reasonable, the $PM_{2.5}$ measurements were compared to 3 other sites in San Diego County operated by the San

Diego Air Pollution Control District (SDAPCD). The average $PM_{2.5}$ measured at the SIO pier during the study (16 $\mu g/m^3$) was similar to the other sites (downtown 10 $\mu g/m^3$, Escondido 18 $\mu g/m^3$, and Alpine 16 $\mu g/m^3$). The downtown San Diego site is the most comparable site to the SIO Pier due to its close proximity and air mass back trajectory patterns. Despite 12 miles separating the SIO Pier and downtown sites, similar trends in $PM_{2.5}$ mass were observed at both sites during the study (**Figure 72a**). This suggests that these transport events described herein likely influence even larger portions of San Diego County.

b. Identification of Regional Events

During sampling at the SIO pier, time periods with high submicron particle concentrations were observed using average hourly submicron (0.5-1 μm) size-resolved particle concentrations from an APS. Trends in submicron ATOFMS particle counts are correlated with submicron APS particle concentrations as shown in **Figure 72b**. The relationship between the APS and ATOFMS submicron counts shows that, despite transmission biases from the ATOFMS inlet, temporal variations in submicron ATOFMS counts directly correspond to changes in atmospheric concentrations (128,337). Multiple time periods showed elevated PM_1 mass concentrations. **Figure 72c** shows PM_1 (blue line) versus $PM_{2.5}$ (red line) mass concentrations calculated using the APS, as described above. The average PM_1 concentration during the study was 7 $\mu g/m^3$ (dashed gray line); this represents an upper limit because certain time periods with low particle concentrations were excluded from the analysis as they did not have the requisite statistics for scaling the ATOFMS counts to mass. Regional events are defined as any period when the peak PM_1 mass was at least twice the average PM_1 concentration (14 $\mu g/m^3$). During regional events, PM_1 accounted for 52% of $PM_{2.5}$ mass and 70% of $PM_{2.5}$ number concentrations.

c. Air Mass History during Regional Events

To determine the source(s) of the submicron particles at the SIO pier, HYSPLIT air mass back trajectories (48 hours) were calculated at 500 meters and patterns were verified by comparing to back trajectories at 200, 400, 600, 800, and 1000 meters (130). Back trajectories calculated for the peak hour of each submicron concentration spike are shown in **Figure 74a**. Many events had back trajectories coming from the vicinity of the LA-LB Port region, while a small number of additional events were more local and passed near the SD Port. These more local events most likely still had contributions from LA-LB transport that stagnated over the region for several days. **Figure 74b** shows air mass back trajectories during nonevent periods. These air masses either came from the west over the ocean or from inland locations but did not pass near the SD or LA-LB Ports.

Figure 74c groups the main air mass back trajectories by type (Port of LA-LB, San Diego, inland, and oceanic) and includes how frequently each type was observed. Back trajectories came from the vicinity of the Ports of LA-LB (32% of the sampling period), the Port of SD (17%), inland (5%), and the ocean (46%). During periods when the air masses came from the LA-LB Port region, regional events were observed 40% of the time. Not all air mass back trajectories coming from the LA-LB port region produced high concentration regional events. In order to create these conditions, high levels of

emissions at the port, consistent boundary layer height, relatively short air mass transport times, and meteorological conditions all have to occur simultaneously. It is important to note that the amount of ship traffic in the LA-LB Port region remained relatively constant (25-40 major ships per day) and thus the major factor contributing to the regional events appears to be proper meteorological conditions (338). Based on the HYSPLIT trajectories, emissions from the Port of SD most likely contributed to two of the events. When oceanic back trajectories occurred, no regional events were observed; this indicates that ship traffic in the open ocean west of San Diego, which is much lower than traffic near the ports, did not contribute significantly to San Diego air quality. During regional transport periods when trajectories came from the LA-LB Port region, it is likely additional sources and processes contributed along the way. Also, the very limited recreational boating in close proximity to the pier and lower ship traffic at the Port of San Diego (1% of LA-LB) leads to lower emissions compared to the Ports of LA-LB and helps explain the lack of events during inland or oceanic time periods (339).

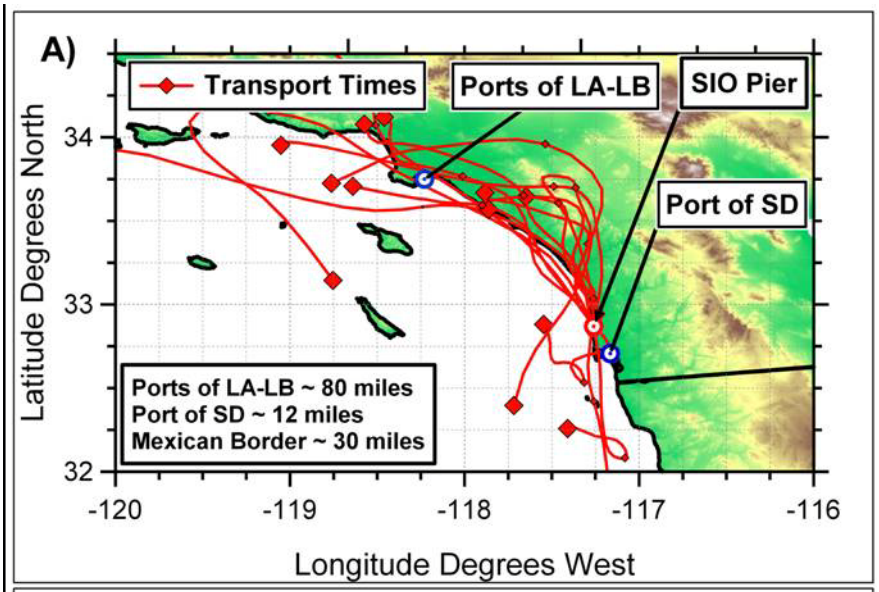

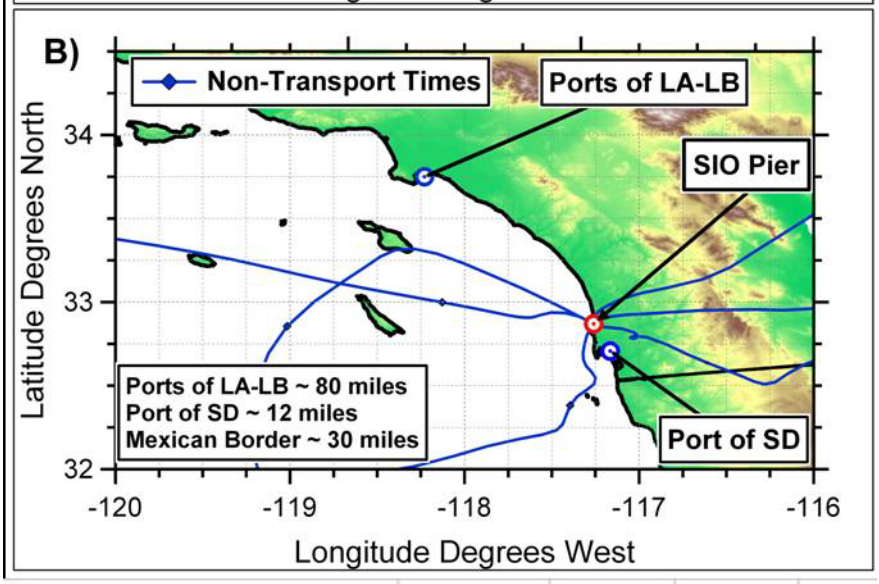

C)

Primary Air Mass Source Region	Port-Coastal	San Diego	Inland CA	Ocean
Transport Type	Regional	Local	Long Range	Mixed
Sample to Source Distance (miles)	77	12	>200	0-500
Fraction of Sampling Time	0.32	0.17	0.05	0.46
Percent Time Submicron Events	0.4	0.29	0	0

Figure 74: HYSPLIT (24 hour) back trajectory analysis at 500 meters for the peak hour of each regional event. Large diamonds represent 24 hours back from the source and small diamonds present 12 hours. A) Trajectories in red pass near the LA Port while trajectories in blue pass over the SD Port. B) Trajectories in purple are representative of non-transport time periods. C) The table included displays the frequency of different air mass types and source regions, as well as the number of regional events observed during each back trajectory type.

d. Particle Chemistry during Regional Transport Events

The most prevalent submicron particle types observed during these regional events were external mixtures of soot, organic carbon, biomass burning, metals, and sea

salt. **Figure 75** shows the average mass spectra of the two most common particle types observed during the regional events. These included an elemental carbon (or soot) particle type mixed with organic carbon, sulfate, nitrate and water, labeled as ECOC(sulfate-nitrate). The second type included vanadium-nickel-iron particles mixed with sulfate, nitrate, carbonaceous species, and water, labeled as V-Ni-Fe(sulfate-nitrate). The particle labeling scheme used herein first indicates the most dominant peaks in the positive ion particle spectra, followed by secondary species detected in the negative ion spectra in parentheses. The positive ion peaks indicate the primary source of the particles, whereas the negative ions provide insight into the atmospheric aging the particles have undergone during transport. Notably, the primary source makes up a high number fraction of particles, but the secondary species make up the bulk of the mass of the particles. The mass spectra of the ECOC(sulfate-nitrate) or soot particles were characterized by elemental carbon cluster ions ($^{12}C_1^+$, $^{24}C_2^+$,…, C_n^+) with less intense organic carbon markers ($^{27}C_2H_3^+$, $^{29}C_2H_5^+$, $^{37}C_3H^+$, and $^{43}C_2H_3O^+$) (81). The V-Ni-Fe(sulfate-nitrate) particle type is characterized by intense peaks at $^{51}V^+$ and $^{67}VO^+$ with less intense iron ($^{56}Fe^+$) and nickel ($^{58,60}Ni^+$) ion peaks. It should be noted that a small percentage of spectra in the other submicron particle types showed minor vanadium and vanadium oxide peaks during these events. These mixtures were most likely formed by coagulation processes, but only represented 2-5% of the total particle spectra.

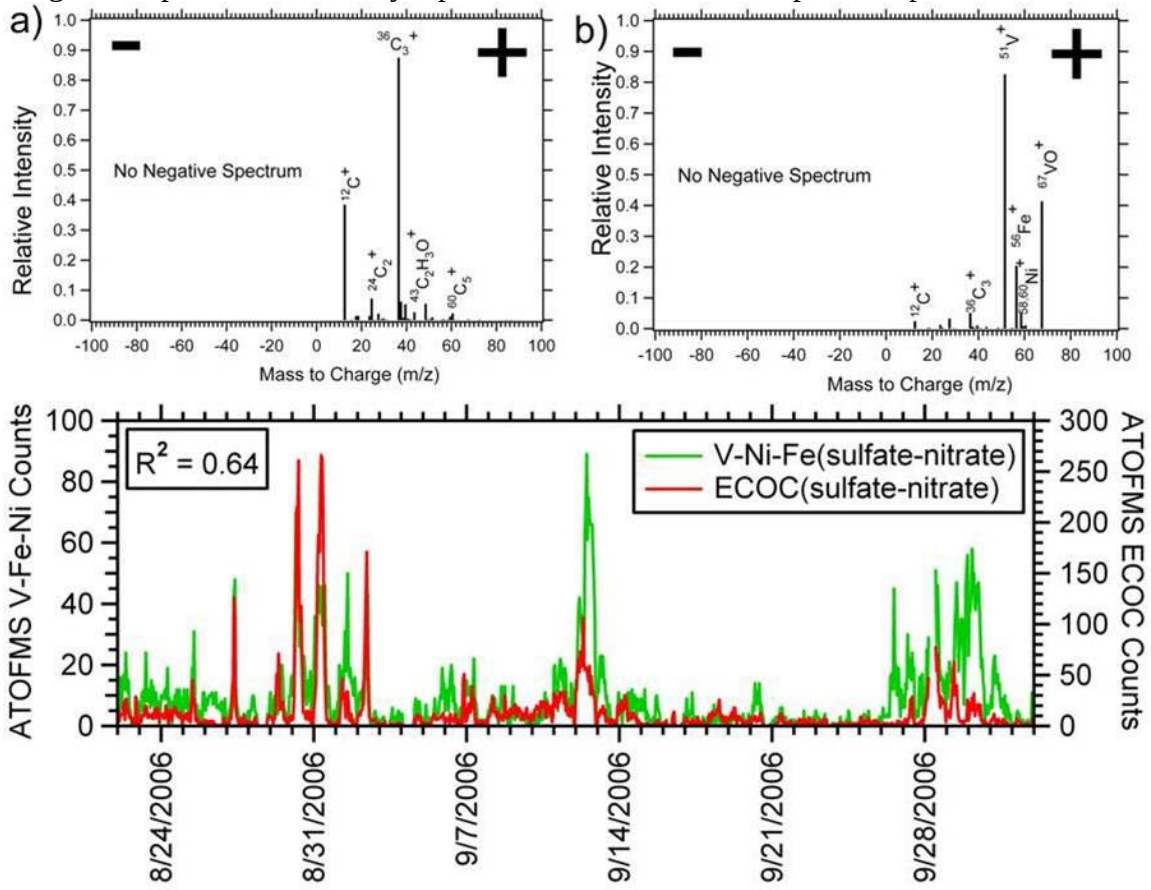

Figure 75: Average negative and positive ion mass spectra for a) ECOC(sulfate-nitrate) and b) V-Ni-Fe(sulfate-nitrate) particles. c) Time series of hourly ECOC(sulfate-nitrate) and V-Ni-Fe(sulfate-nitrate) particle type counts.

e. General submicron particle types

Average mass spectra of each particle type (beyond ECOC(sulfate-nitrate) and V-Ni-Fe(sulfate-nitrate)) are shown in **Figure 76** and described below. Elemental carbon particles were identified by carbon cluster ions ($^{12}C_1$, $^{24}C_2$,…, C_n) as the dominant peaks in the positive and negative ion mass spectra, as well as sulfate and nitrate ions ($^{97}HSO_4^-$, $^{62}NO_3^-$, and $^{46}NO_2^-$), markers that are associated with aging (81). Organic carbon particles have intense ion markers at $^{27}C_2H_3^+$, $^{29}C_2H_5^+$, $^{37}C_3H^+$, and $^{43}C_2H_3O^+$ (81). Biomass burning particles have a dominant potassium peak ($^{39}K^+$), as well as elemental and organic carbon marker ions. This particle type also has a significant sulfate ion peak ($^{97}HSO_4^-$) and a minor $^{213}K_3SO_4^+$ peak (not shown) which has been linked previously with biomass burning (87,162). Sea salt particles were identified by $^{23}Na^+$, $^{62}Na_2O^+$, $^{63}Na_2OH^+$, and $^{81,83}Na_2Cl^+$ (337). Sea salt with soot particles were characterized by an intense $^{23}Na^+$ peak, elemental carbon cluster ions, organic markers, and other sea salt ion peaks (m/z 62, 63, 81, and 83). This particle type is formed from coagulation of SS and ECOC particles during transport (337,340).

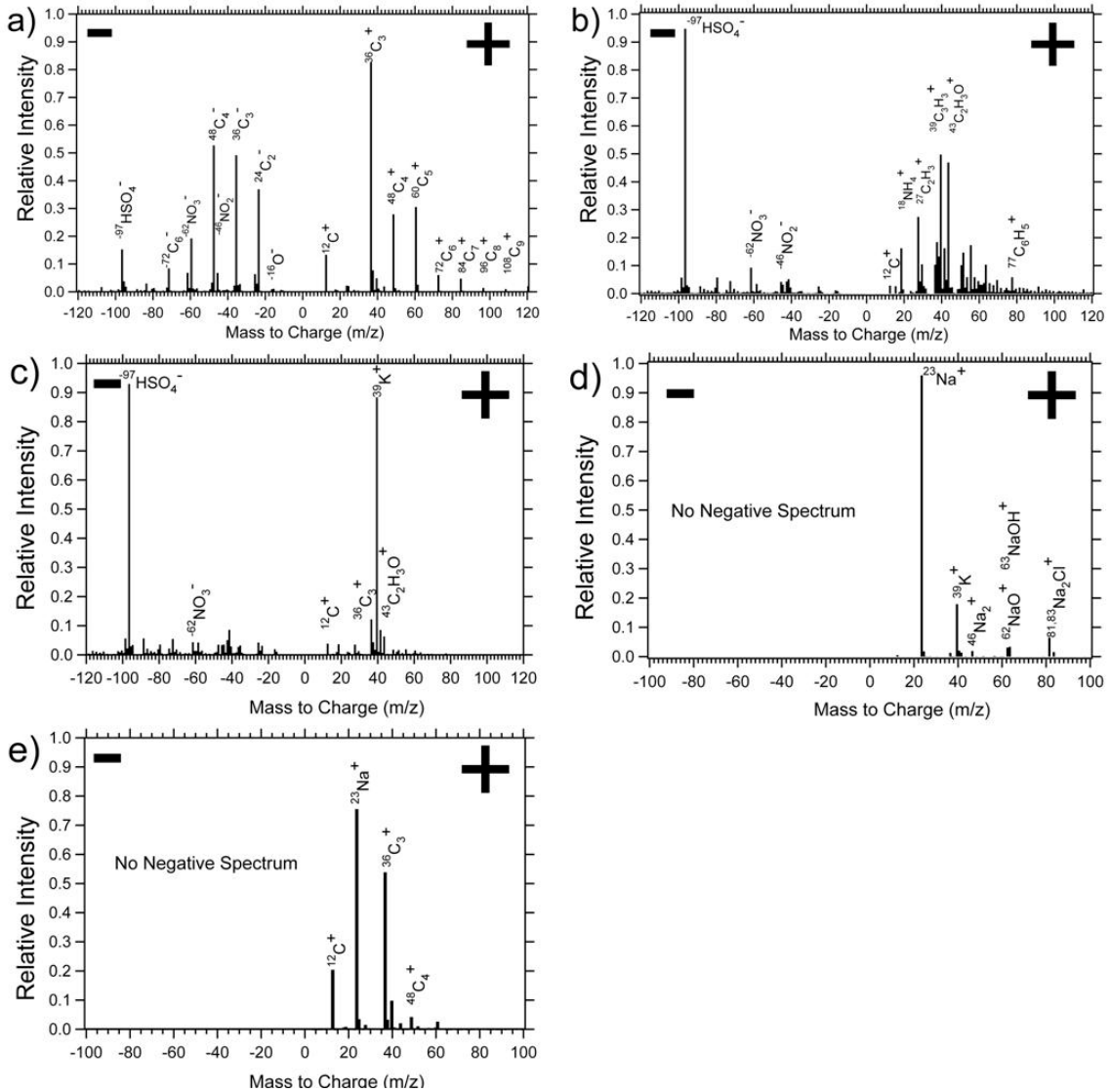

Figure 76: Average negative and positive ion mass spectra for the top six particle types (excluding ECOC and V-Ni-Fe which are discussed in the main paper): a) Elemental carbon, b) Organic carbon, c) Biomass Burning, d) Sea salt, e) Sea salt with soot.

f. Sulfate Formation and Aging Processes During Transport

It is important to note that a high percentage (30-80%) of particles did not produce negative ion mass spectra. Based on optical measurements of single particles with similar chemical signatures (129), water has been shown to remain on the particles which can suppress negative ion formation (82,341). The larger (0.5-1 μm) size of these particles also suggests they have undergone a significant amount of chemical aging during transport. The aging processes include condensation of secondary species, aqueous phase processing of SO_2, as well as coagulation with pre-existing sulfate marine background particles (158).

Due to high SO_2 concentrations in the port region coupled with high average ambient relative humidity (~93%), it is likely that the particles acquired sulfate due to SO_2 oxidative processing when initially formed. In addition, the particles most likely picked

up additional secondary species (sulfate and nitrate), water soluble organic carbon, and water during transport. This is supported by the fact that for both particle types, the limited particles with negative ion mass spectra showed a major bisulfate ion peak ($^{97}HSO_4$), as well as nitrate ion peaks ($^{46}NO_2$ and $^{62}NO_3$). The observations from this study, along with a previous study in the southern California coastal region showing marine background particles with high levels of sulfate, suggest that the ECOC and V-Ni-Fe particles are likely composed of relatively small primary particle cores mixed with sulfate, nitrate, and water (158). Similar observations in previous studies of single soot particles, where core sizes of less than 0.2 μm were observed (84), show that sulfate and nitrate species contribute the majority of the mass to these aged particles. Previous work has also shown that sulfate is associated with ship emissions at the source (61,79). Concurrent filter-based triple oxygen isotope measurements of sulfate at the SIO Pier estimate that ships represent 10-44% of non-sea salt sulfate mass concentrations below 1.5 μm (342). These co-located isotope measurements also suggest the ECOC(sulfate-nitrate) and V-Ni-Fe(sulfate-nitrate) particles acquired significant quantities of sulfate and water at the point of emission as well as through secondary aging processing during transport.

g. Temporal Variations by Particle Type

Figure 77 shows the scaled a) relative fractions and b) contributions to PM_1 mass of the different submicron particle types by hour throughout the study. The black line shows the hourly PM_1 mass concentrations ($\mu g/m^3$). The particle type representing the majority of submicron mass varies strongly with the concentration of submicron mass. When PM_1 levels were high (>14 $\mu g/m^3$), soot and V-Ni-Fe particles account for 24-86% (52% average) of submicron mass. Sea salt, the primary background submicron particle type, represented a significant fraction of submicron particles (75-80%) during periods when the lowest PM_1 mass concentrations were observed and PM_1 was the smallest fraction of $PM_{2.5}$. These represent marine background periods with high wind speeds. Biomass burning and organic carbon showed low correlations with PM_1 ($R^2 = 0.09$ and $R^2 = 0.11$), suggesting these particle types did not come from the same sources as most of the submicron particles detected at the pier.

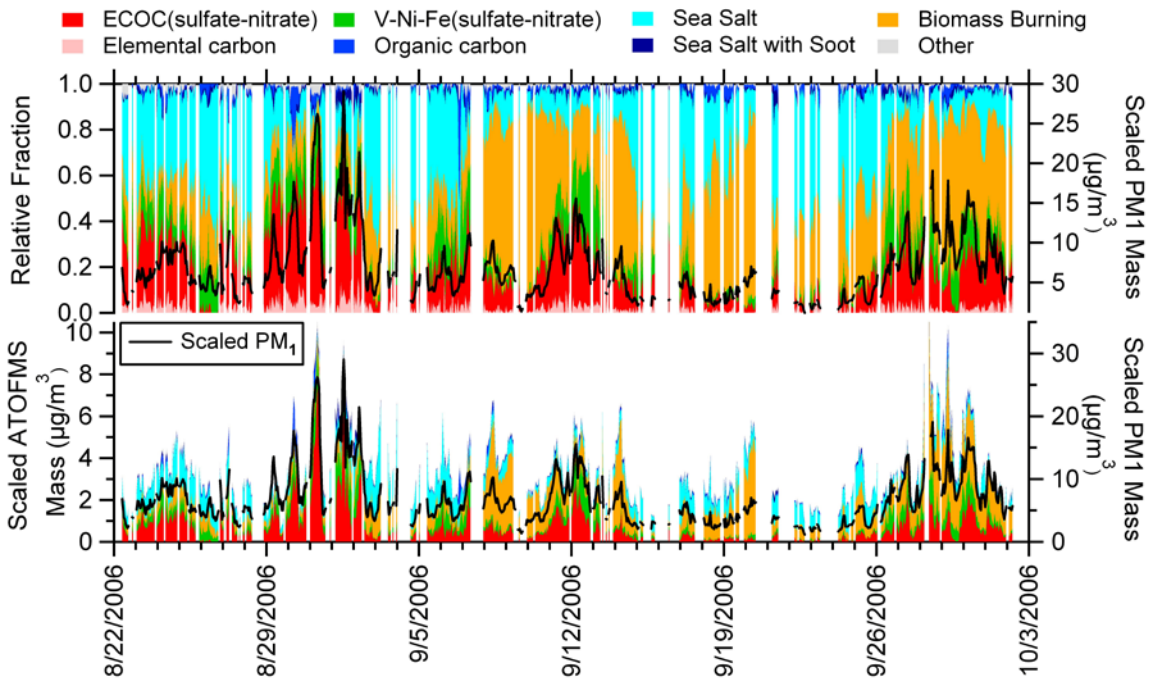

Figure 77: a) Time series of the relative fractions of submicrometer particles types b) Time series of counts of submicron particle types. The black line on both plots is the scaled PM_1 mass concentration ($\mu g/m^3$).

h. Correlation between Major Particle Types

Metal-containing particles composed of trace amounts of V, Fe, and Ni mixed with carbonaceous species are primarily emitted from residual fuel combustion processes and as such have limited sources, including ships and refineries (73,343). Since no refineries exist in San Diego or Orange County and residual fuel is burned only on large ocean going vessels, this limits likely sources to ships from the Ports of LA-LB and Port of SD, as well as refineries near the Ports of LA-LB. ECOC particles represent a general type produced by most combustion sources, including diesel truck and automobile emissions (36,344); however the larger sizes observed (> 0.5 μm) and low percentage of particles with negative ion mass spectra, indicate that the particles were highly aged and not from local vehicle sources. **Figure 75c** shows the high correlation (R^2 = 0.64) observed between the number concentrations of V-Ni-Fe(sulfate-nitrate) particles and ECOC(sulfate-nitrate) particles with one hour resolution. Ships burn a variety of fuels (i.e. distillate and residual) that produce the soot and V-Ni-Fe(sulfate-nitrate) particle types in different proportions (79,345), that depend on the type of engine, fuel, and operating conditions. The temporal correlation of the V-Ni-Fe(sulfate-nitrate) and ECOC(sulfate-nitrate) particle types (**Figure 75c**) and the significant contributions to PM_1 mass (**Figure 78**) during regional events suggests that these two particle types originate from the same source and/or source region. The Supporting Information shows one specific event where a strong correlation between the mass concentrations of ECOC(sulfate-nitrate) and V-Ni-Fe(sulfate-nitrate) for a regional event and the number of ship radio contacts for that period. This occurred during the period with the most rapid (6 hours) transport from the LA-LB Port to the pier. In general, the number of ship

counts in the LA-LB Port region was relatively constant. As described, meteorology, rather than a change in source emissions, appeared to control the high concentrations and regional events observed at the SIO Pier during this study.

i. Size-Resolved Chemistry of Regional Events

The size-resolved chemical mass distributions, calculated using the APS method discussed above, are shown for the average of regional events (**Figure 78a**) as well as the average of non-event time periods for comparison (**Figure 78b**). Regional events showed higher mass concentrations across all submicron sizes (4.7-6.5 μg/m^3) when compared to non-event time periods (2.9-3.8 μg/m^3). During regional events, the ECOC(sulfate-nitrate) particles represent the most significant fraction of submicron mass in each bin (35-44%), while V-Ni-Fe(sulfate-nitrate) particles contribute 10-19% of particle submicron mass. Note that this is a unique single particle perspective of the mass fractions, and it focuses on the mass fraction of the entire particle type. As previously noted, the majority of the mass of these particles was most likely sulfate, nitrate, and water, as well as a smaller amount of carbonaceous species from residual oil and secondary organic carbon. Soot mixed with sea salt, which has been observed in previous studies during long range transport episodes, showed higher mass concentrations during the event periods (340). These particles were most likely formed by coagulation processes occurring during the longer transport periods. Non-event time periods had much lower ECOC(sulfate-nitrate) (4-22%) and V-Ni-Fe(sulfate-nitrate) (2-10%) mass fractions, showing significantly higher fractions of background particle types. These background types included more sea salt (16-81%) and biomass burning (9-43%) than sea salt (4-28%) and biomass burning during (11-28%) regional events. During these periods, PM_1 mass represents only 36% of $PM_{2.5}$ compared with 60% during regional events. The increase in the overall PM mass and contributions from ECOC(sulfate-nitrate) and V-Ni-Fe during regional events shows the major influence of transported emissions on San Diego air quality. Notably, these transported aerosols (ships, refineries, and port vehicle traffic) make much higher contributions to PM concentrations than local San Diego sources during these events.

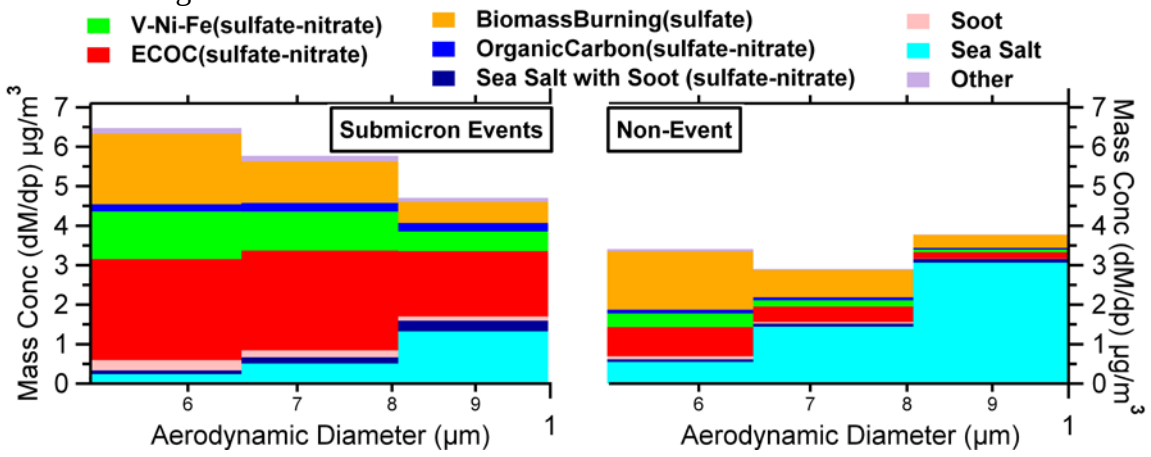

Figure 78: Comparison of the average size-resolved mass distributions of major particle types during regional events and non-events.

i. Correlation between Ships at Sea and Selected Particle Types

Radio transmissions of the location, speed, and heading were recorded in real time for ships in Southern California waters with an automated identification system (AIS) antenna in La Jolla, CA and binned as the number of transmissions per hour (75). These transmissions are required for ships at sea over 299 gross tons every minute by the International Maritime Organization (IMO). **Figure 79** shows one major regional transport event, based on HYSPLIT back trajectories, from September 12-13 with the black line representing the number of recorded ship positions per hour. The transport time from the LA-LB port region during this particular event was ~6 hours and the peak in radioed positions occurred roughly 5-7 hours before the peaks in V-Fe-Ni and ECOC particles, suggesting ships were a contributor to the increase in particle concentrations. To observe this strong correlation required many conditions including favorable meteorology, air mass direction and speed, meteorology favorable to radio transmissions, and a sharp spike in the number of ships at sea. This correlation occurred only one time during sampling, but provides further evidence that the LA-LB port region is a significant source of PM in San Diego.

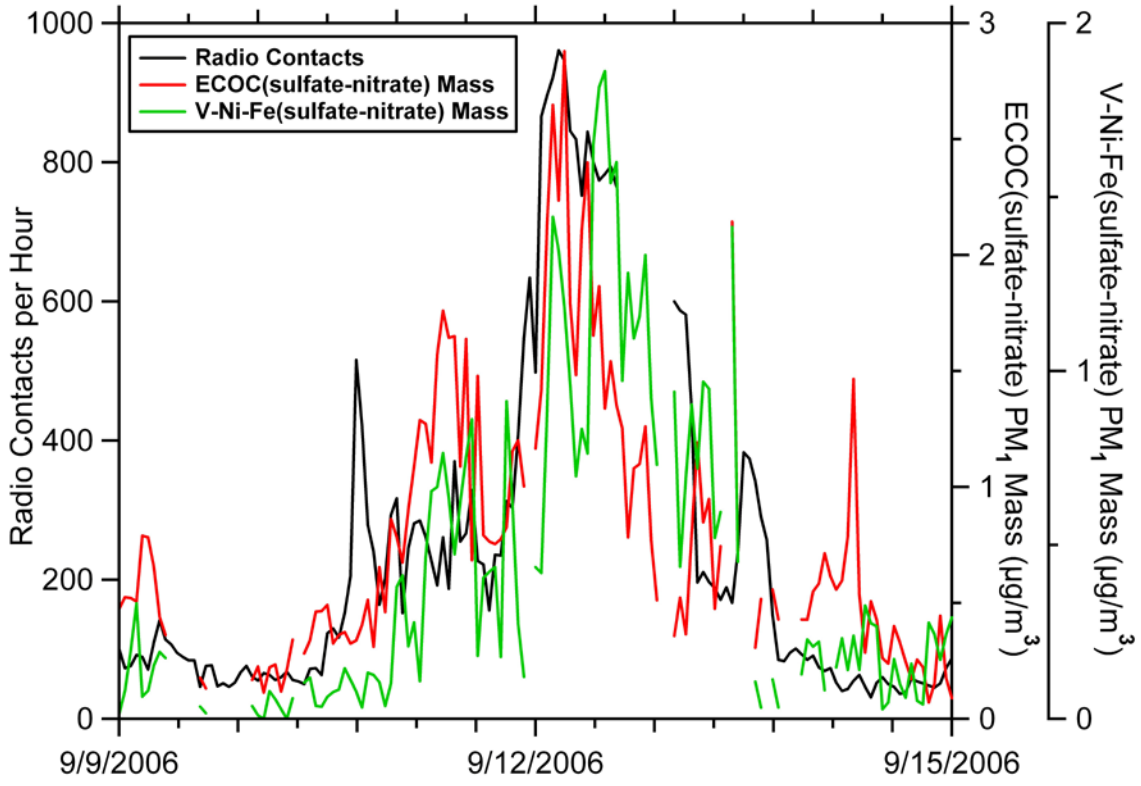

Figure 79: Time series of hourly counts of the ECOC and V-Fe-Ni particle types during 6 day period with ship positions recorded per hour.

j. Impact of Regional Events

Regional transport periods resulted in PM_1 mass concentrations that were increased by a factor of 2-4, showing how strongly ships, refineries, vehicles, and other port combustion sources from the Ports of Los Angeles and Long Beach impact air quality in the San Diego area. Emissions transported 12 miles north from the Port of San Diego, while less frequent, most likely mixed with regionally transported emissions and

play a role in lowering the overall air quality of the San Diego region. Particles between 0.5-1 μm contribute the most mass to PM_1 and $PM_{2.5}$ for the regional events. The majority of the mass for these particles is likely a mixture of sulfate, nitrate, and water, but identifying the core (ECOC or V-Ni-Fe) is critical to identifying the original particle source and allowing the proper regulations to be established. The adverse health effects of residual fuel combustion particles, which contain a complex mixture of carbonaceous and metals, on residents of San Diego county as well as other coastal cities could be quite significant (64).

Long-term sampling at a coastal site with speciated aerosol number and mass concentration measurements will shed further light on the frequency and intensity of these transport periods and how they vary seasonally. The impact of regionally transported pollution on receptor site locations beyond San Diego needs to be considered when evaluating the health impacts of particles in urban and rural areas. These emissions will become even more important as vehicle emissions become further regulated and residual oil sources such as shipping continue to grow. The strong influence of regional transport on San Diego air quality in comparison to the impact of local emissions demonstrates the importance of monitoring and further regulating these sources in the future.

iv. Acknowledgements

The authors gratefully acknowledge Dr. Gerardo Dominguez and Prof. Mark Thiemens for providing the ship tracking data. The authors acknowledge and thank Dr. Ryan Sullivan, Lindsay Hatch, Margaret Yandell, Elizabeth Fitzgerald, and John Holecek for their support and assistance with measurements at the SIO Pier. William Brick at the San Diego Air Pollution Control District is thanked for sharing San Diego County $PM_{2.5}$ mass concentrations. Funding was provided by the California Air Resources Board under contracts 04-336 and 05-346. The authors gratefully acknowledge the NOAA Air Resources Laboratory for the provision of the HYSPLIT transport model and READY website (http://www.arl.noaa.gov/ready.html) used in this publication.

11. Single Particle Composition, Hygroscopicity, and CCN Activity during the 2007 San Diego Wildfires

i. Introduction

Biomass burning can be a significant source of aerosols in many regions of the world (346). Biomass burning aerosol particles (BBA) are a common component of tropospheric aerosol and have been observed to varying degrees in several locations with various techniques including Proton-Induced X-ray Emission (PIXE), Scanning Electron Microscopy (SEM) and single particle mass spectrometry (SPMS) (346-352). Since most of BBA are smaller than 400nm(351,353,354), their removal from the atmosphere is not dominated by dry deposition, but preferably by cloud droplet activation and wet deposition (355). BBA can also become transported to high altitudes and undergo long range transport, affecting global climate (348,356,357). Risk of wildfires is an increasing concern because of increased dryness in certain regions due to climate change (358). Smoke and pollution aerosol can either increase or decrease cloud cover through indirect effects by modifying cloud microphysics, and can directly alter radiative transfer by absorbing and reflecting radiation. These aerosol-climate feedbacks are some of the largest uncertainties in climate research (359-364). Biomass burning can cause intense convection, where the aerosol is transported to high levels in the atmosphere (365). The resulting large updraft velocities can produce high water supersaturations and thus cause the BBA to nucleate cloud droplets.

Due to the abundance, cloud interactions, and wet removal of BBA, it is especially important to understand its interaction with water. Uptake of water by aerosols is determined by their chemical content and thus hygroscopicity, and interactions with water can in turn alter their physical and chemical properties (366). Water content can alter the partitioning of semi-volatile species between the gas and particle phases, which further effects aerosol composition (367) and aqueous chemistry (368). Hygroscopicity strongly influences the light scattering, cloud condensation nuclei (CCN) activity, refractive index and size of aerosols. These properties are essential for understanding the aerosol direct and indirect effect on the global radiation budget (358,362).

An important factor determining the composition of BBA is fire type, fuel type, and age of the smoke (369,370). Flaming fires (pyrolysis) tend to produce particles with higher inorganic content and more elemental carbon, while smoldering fires (charring) tend to produce more organic carbon rich aerosol (351,354,371-374), which include water-soluble sugars such as levoglucosan. If the particles contain relatively little inorganic salts that can absorb water, they may exist as tarballs (353). In fact, it has been shown that fire type is more important than fuel type for chemical signatures of the resulting particles (375), while others have shown large differences in chemical signatures with both fire type and fuel type (374). In general, the carbon content of the fuel is a limited range (~37-54%), therefore emission factors are a function of combustion conditions for carbon, oxygen and hydrogen containing compounds (376). Other minor elements like nitrogen, sulfur and the halogens emission factors depend on the concentrations in the fuel and combustion conditions(376). The large fractions of soluble inorganic and organic compounds can make BBA hygroscopic and thus efficient CCN (368,377), and some of these organic compound are hygroscopic enough to cause cloud

droplet activation without the association of inorganic compounds (377). Previous studies have shown that knowledge of the contribution of water soluble organic carbon (WSOC) is essential to predicting the hygroscopicity of ambient aerosol (365,378-380). Using filter extractions of biomass burning aerosol, (381) have shown that hygroscopicity depended on the type of biofuel. A wide range of hygroscopicities (κ = 0.06-0.7) was measured from a variety of biomass materials that were strongly dependent on fuel type (370).

Fresh biomass burning particles, consisting of mostly potassium, chloride, and organic carbon(382,383), can be readily converted to potassium nitrate (KNO_3) and potassium sulfate (K_2SO_4) via heterogeneous reactions with secondary acids such as HNO_3 and H_2SO_4 during atmospheric transport (371,384-386). These heterogeneous reactions have important implications for BBA hygroscopic properties, as the deliquescence relative humidity (DRH) of K_2SO_4 and KNO_3 are 97.4 and 92.5%, respectively, while KCl is 84.3% (371); as well as releasing chlorine gases to the atmosphere.

During the fall 2007 wildfires in San Diego, over 2,000 homes and 300,000 acres were burned in San Diego County for a total of 3069 homes and 516,465 acres in all of Southern California (387). Particle number concentrations were 10 times higher than normal background (36,748 ± 21,646 particles cm^{-3}), especially for particles with diameters < 300nm. In this study we compare CCN concentrations and aerosol hygroscopicity with submicron single-particle size and chemical composition in various air masses during October and November 2007 to investigate the different factors that influenced aerosol chemical composition and their resulting hygroscopicity during a period heavily influenced by biomass burning.

ii. Experimental

a. Sampling locations and instrumentation

Ambient particles were sampled from outside the laboratory on the second floor of Urey Hall (32°52’31.66”N, 117°14’28.64”W) on the campus of the University of California, San Diego (UCSD) from Sunday, October 21 to Thursday, November 1, 2007. The aerosol was sampled through a 3/8” stainless steel tube that extended outside through the exterior wall, and delivered to the various instruments. The lab is located approximately 1 km from the Pacific Ocean coastline at an elevation of ~130 m above sea level. Single particle aerodynamic size and chemical composition were measured in real-time with an ultrafine aerosol time-of-flight mass spectrometer (UF-ATOFMS) instrument equipped with an aerodynamic lens that transmitted an aerodynamic diameter (D_a) size range of 50 to 300nm. Single particles are sized based on their time-of-flight between two 532 nm CW lasers and then ablated and ionized by a Q-switched 266 nm Nd:YAG laser. The resulting positive and negative ions are analyzed by a dual-polarity reflectron time-of-flight mass spectrometer. Further details on the UF-ATOFMS instrument design and operation are described elsewhere (388). The particle size distributions and number concentrations were measured concurrently by a scanning mobility particle sizer (SMPS, TSI Model 3936) with sheath and aerosol flows of 4.0 and 0.4 lpm, respectively. CCN concentrations were measured with a streamwise thermal-gradient CCN counter at a supersaturation of 0.29% (389). The instrument was calibrated

before use with ammonium sulfate aerosol (99.999%, Sigma Aldrich). Total particle condensation nuclei (CN) concentrations were measured with a condensation particle counter (CPC, TSI model 3007). The fraction of CCN active particles, or fCCN, was obtained from the CCN/CN ratio. A second CCN counter and CPC (TSI model 3010) was located at the Scripps Institution of Oceanography (SIO) Pier (32° 51'47.232"N, 117° 15'21.6"W) and operated at a supersaturation of 0.13%. The sampling setup on the SIO Pier was approximately 50 feet above sea level and a quarter of a mile from the coast. We will refer to the Urey Hall CCN as CCN_0.3 and the SIO Pier CCN as CCN_0.1. Meteorological data was also obtained from the SIO pier.

b. ATOFMS data analysis

The UF-ATOFMS single particle data were automatically sorted and grouped into clusters of particles with similar mass spectral characteristics using the adaptive resonance theory neural network algorithm, ART-2a. The main user-defined parameters for ART-2a are the learning rate, number of iterations, and vigilance factor, which were set to 0.05, 20, and 0.85, respectively (390). The resulting clusters were then analyzed manually and classified into distinct particle types based on their mass spectral features(348,350,391-393). The dual polarity (having both positive and negative ion spectra) biomass clusters were combined to yield the subset of particles presented herein. We have observed no significant change in average chemical marker peak areas as a function of vacuum aerodynamic diameter 50-300nm on the BBA.

c. Single hygroscopicity parameter

To summarize the hygroscopicity measurements made with the CCNcs, a single parameter for particle hygroscopicity (κ) is used (394). The following equation defines the relationship between a growing particle's equilibrium water saturation ratio, S, diameter, D, dry diameter, D_{dry}, and hygroscopicity, κ:

$$S(D) = \frac{D^3 - D_{dry}^3}{D^3 - D_{dry}^3(1-\kappa)} \exp\left(\frac{A}{D}\right) \qquad (1)$$

where A = 2.1x10^{-9} m is a constant evaluated for a surface tension of 0.072 J m^{-2} (pure water) and temperature of 298.15 K (394). κ describes a particle's water activity and typical values range from 1.4 (hygroscopic soluble salt) to about 0 (insoluble but wettable) for atmospherically relevant systems. Plotting the critical supersaturation of identical particles of varying size in log s_c – log D_{dry} space yields kappa isolines where particles lying along one isoline will all have the same hygroscopicity (κ). The CCN activation diameter (D_{act}) of atmospheric aerosols at s = 0.29% (CCN_0.3) and s = 0.13% (CCN_0.1) was estimated using the measured size distributions, CN, and CCN concentrations. D_{act} was derived by

$$1 - \frac{CCN}{CN} = \frac{\int_{D_0}^{D_{act}} n(D)dD}{N_{total}} \qquad (2)$$

where N_{total} is the cumulative concentration obtained by integrating the observed size distribution of $n(D)$, D is the electric mobility diameter selected by the SMPS and D_o the smallest size measured by the SMPS (~11 nm). The CCN/CN ratio represents the fraction

of the CCN-active aerosols (fCCN). Therefore, the quantity 1-CCN/CN represents the fraction of non-CCN active aerosols. Eqn. (2) assumes that all chemical compositions are internally mixed (i.e. one particle composition). This approach was taken to simplify the data analysis and still reflects how much the relative degree of variation in the chemical composition affects CCN activity, as the size resolved chemistry was measured (391). We have estimated an approximate relationship between D_{act} and κ to be $D_{act} \sim \kappa^{-1/3}$(395). In the estimation of D_{act}, contributions from particles larger than the range of the SMPS (upper range = 600 nm for our settings) were not considered, but were most likely relatively quite low and made minor contributions to the total aerosol concentration as biomass particles are primarily less than 400 nm (354).

iii. Results and Discussion

This study can be described by five different time periods based on the Urey Hall laboratory-based CCN and fCCN (from now on referred to as CCN_0.3, fCCN_0.3), size distributions, particle chemistry and air mass back trajectories. HYSPLIT air mass back trajectories during different time periods are displayed in **Figure 80**. A summary of time periods and their CCN, fCCN, CN, size distributions, particle chemistry and HYSPLIT is provided in **Table 13** and **Table 14**.

Period Name/time	fCCN_0.3	NCCN1_0.3	CN_0.3	Kappa_0.3	SMPS	Biomass Particle Chemistry	HYSPLIT
1. Santa Ana Fire 10/22-10/23	0.36 +/- 0.09	7448 +/- 4453	21984 +/-17906	0.05 +/-0.05	125 nm (11.8/209.1)	Larger inorganic signatures	Strong Santa Ana
2. 10/24-10/25 12:00 Local stagnation	0.34 +/- 0.11	4114 +/- 1531	12495 +/-3485	0.04 +/- 0.008	150 nm (25.9/209.1)	Small increase in ammonium	Stagnated; from ocean and inland
3. 10/25 12:00-10/26 12:00 1st Ammonium Period	0.36 +/- 0.10	4013 +/- 1208	11047 +/-2578	0.05 +/- 0.02	190 nm (27.9/299.6)	Large increase in ammonium	From ocean
4. 10/26 12:00-10/28 00:00 2nd Ammonium period	0.17 +/- 0.06	1195 +/- 243	7570 +/- 2627	0.03 +/- 0.008	60 nm (15.1/278.8)	Ammonium signal still high	From coast, ocean, inland
5. 10/31 12:00- 11/1 12:00 Local background	0.20 +/- 0.09	1035 +/- 275	10038 +/-13227	0.06 +/-0.03	20nm (14.6/117.6)	Many particle types; none specifically tracking CCN	From North along coast

Table 13: Overview of different Urey Hall CCN periods based on CCN activity, size distributions, particle chemistry and hysplit back trajectories (see dividing lines in **Figure 81**). SMPS data is the average mode for that period with the min/max mode of $dN/dlogD_p$ in parenthesis.

Period Name/time	fCCN_0.1	NCCN2_0.1	CN_0.1	Kappa_0.1*
1. Santa Ana Fire 10/22-10/23 a; b	0.60 +/- 0.15	9600 +/- 5974	15477 +/- 6896	0.5 +/- 0.4
2. 10/24-10/25 12:00 Local stagnation	0.47 +/- 0.13	4567 +/- 1437	9941 +/- 1948	0.3 +/- 0.08
3. 10/25 12:00- 10/26 12:00 1st Ammonium Period	0.53 +/- 0.08	4267 +/- 990	8160 +/- 1843	0.4 +/- 0.4
4. 10/26 12:00- 10/28 00:00 2nd Ammonium period	0.33 +/- 0.15	1610 +/- 446	5641 +/- 2136	0.3 +/- 0.1
5. 10/31 12:00- 11/1 12:00 Local background	0.39 +/- 0.11	1177 +/- 352	3106 +/- 722	0.5 +/- 0.3

Table 14: Overview of SIO Pier CCN, fCCN, CN and Dact during Urey Hall CCN periods (from table 1a).

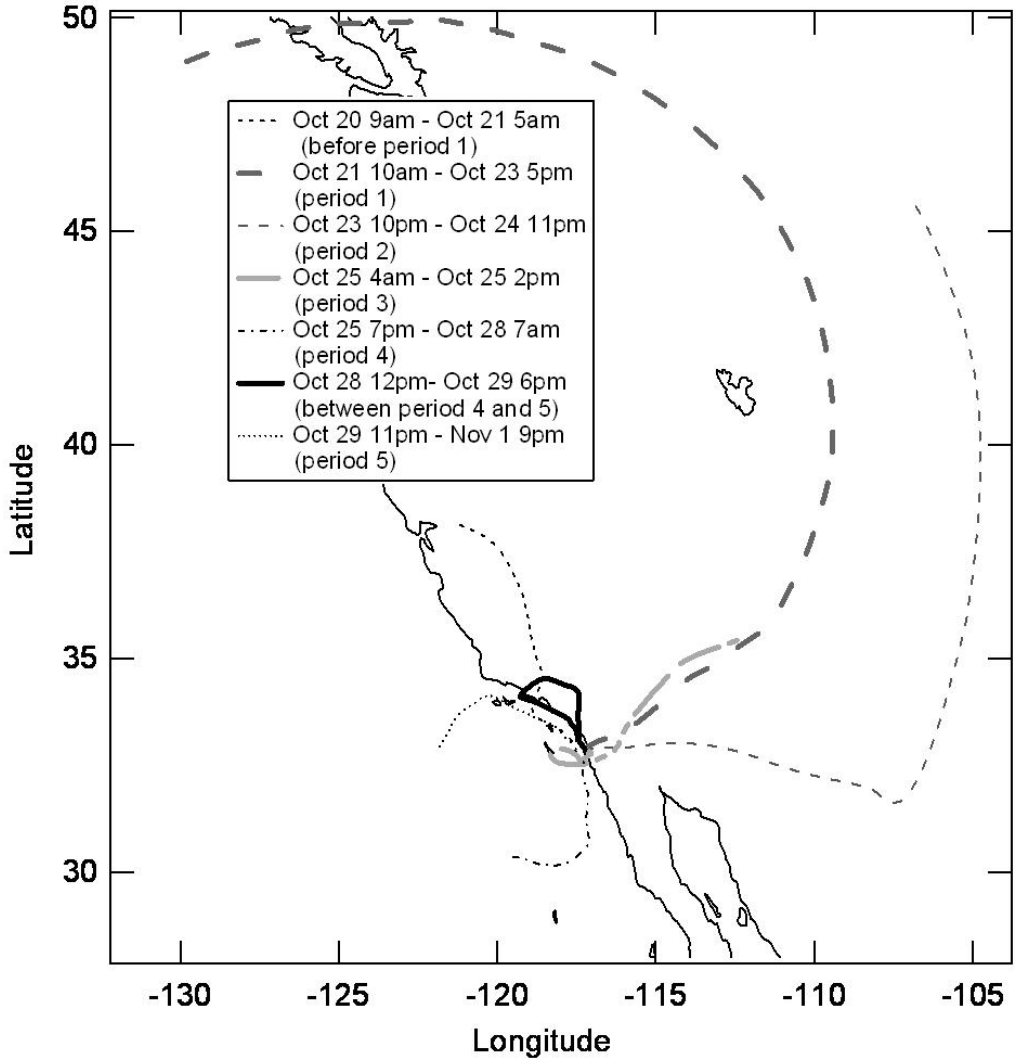

Figure 80: HYSPLIT back trajectories during wildfire sampling period. Each line is a representative 48 hour backtrajectory during that period at 500m. Corresponding periods for comparison to sampling data are in parenthesis.

a. Temporal trends of UCSD CCN_0.3, UCSD CN

Period 1, Santa Ana fire, was dominated by Santa Ana winds and had UCSD CCN_0.3 concentrations up to 14,000/cm^3 and UCSD CN concentrations up to 58,000/cm^3. Period 2, local stagnation, was dominated by air stagnated over the inland region; period 3 by high ammonium content in the particles and air masses from the ocean; period 4 also by high ammonium content and air from the coast and ocean; and period 5 by local coast/ocean air masses. Typical background CN concentrations are 5,000-10,000/cm^3, as were observed during Period 5. As shown in **Figure 81**, CCN_0.3 and CN counts were very high (>10,000) during the Santa Ana fire period. The fraction of CCN_0.3, or fCCN_0.3 (UCSD CCN_0.3/UCSD CN) was also high (0.23-0.47) during the Santa Ana fire period (period 1). Overtime, going from period 1 to period 4 there is a gradual decrease in both CCN_0.3 concentrations, and fCCN_0.3 with notable spikes in fCCN_0.3 along the way. During the first ammonium period (period 3), there is a large increase in UCSD fCCN_0.3 from 0.2 to 0.5. There is also a large increase in relative humidity (RH) during this period.

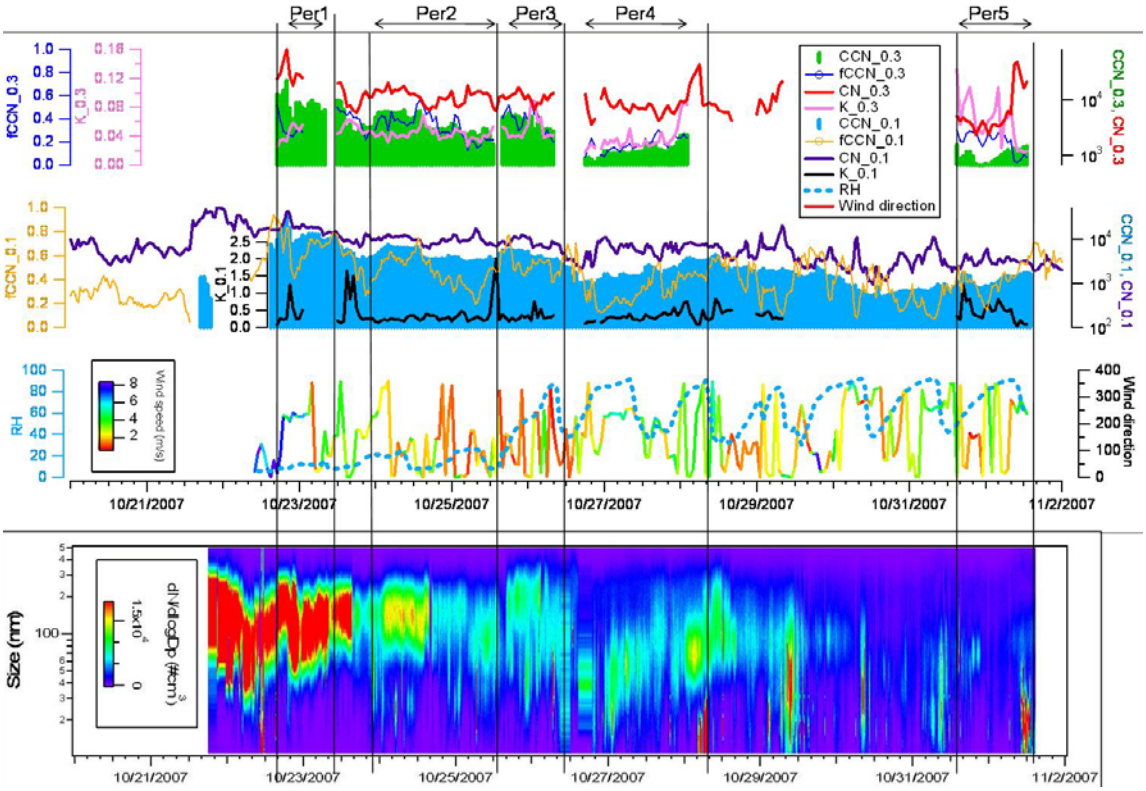

Figure 81: Overview of Urey Hall CCN (UCSD CCN_0.3) and SIO CCN (SIO CCN_0.1) concentrations (s=0.29, 0.13 respectively), fCCN_0.3, fCCN_0.1, Dact_0.3, meteorological data and Urey Hall SMPS

b. Composition, size and CCN

Single particle size and chemical composition was measured concurrently with fCCN_0.3. As the majority of BBA are < 400 nm (353,354), by comparing the composition of particles at these sizes will help determine the relationship between particle size, chemistry and hygroscopicity that control D_{act}. As shown in **Figure 82**, the majority (70-95%) of the particles during periods 1 through 3 were BBA. After period 3, other particles types including elemental carbon and amines had an increased contribution (30-60%) to the total particles < 300nm. Period 5 occurred well after the fires ended began and represents more typical background conditions in the San Diego area (**Figure 81** and **Figure 82**). The SMPS size distribution (**Figure 81**) shows that during the Santa Ana fire period, the BBA dominated (**Figure 82**) and had a mean diameter around 125 nm (**Table 13**).

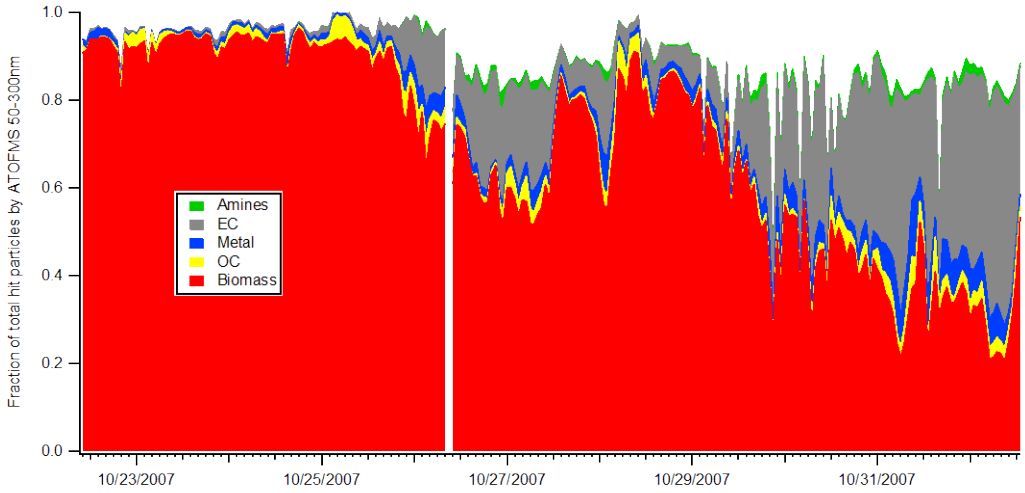

Figure 82: Particle classification temporal. Shown is the classification of particles detected between 50 and 300 nm by the ATOFMS during the study. Biomass is shown in red and is the dominant type during most of the period. Gray is elemental carbon (EC) and grows in as biomass decreases.

Using single-particle mass spectrometry in real time with an ATOFMS allows us to track single-particle mixing state with high time resolution. Each particle that is ionized via laser desorption gives both a positive- and negative-ion mass spectrum. During this study the dominant submicron particle type between 50-300 nm was biomass. The ATOFMS has previously been used to determine biomass burning markers from Southern California biota (393). Fine particle potassium with carbonaceous signatures are known to be markers for biomass combustion (347,354,371,393,396). The concentration of potassium can range depending on the type of fuel. It has been shown that both sulfate and nitrate can be internally mixed with potassium in biomass burning single particles produced from flaming fires (393). Levoglucosan has also been used as a marker for biomass burning (397). Due to the variability in the laser desorption process, we cannot be strictly quantitative, but due to the relatively constant ionization matrix of the BBA particles, we can look at relative abundances of various chemical species by tracking their peak areas on a specific particle type. Main ion peaks used in this manuscript are: NH_4 (m/z +18); K (m/z +39); $(C_2H_5)_2NCH_2$ (m/z +86); $(C_2H_5)_3N$(m/z +101); Cl (m/z -35); CHO_2 (m/z -45); NO_2 (m/z -46); CH_3CO_2 (m/z -59); NO3 (m/z -62); $C_3H_3O_2$ (m/z -71); $CH_3CH_2CHO_2$ (m/z -73); SO_3 (m/z -80); CH_3COCO_2 (m/z -87); $COOHCO_2$ (m/z -89) and HSO_4 (m/z -97).

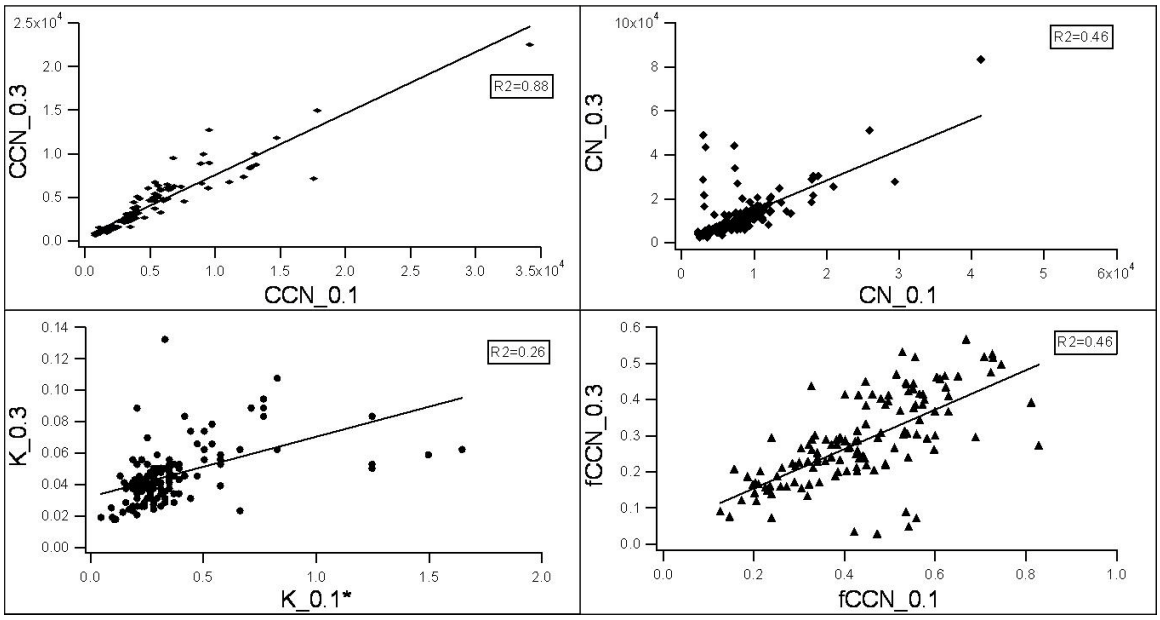

Figure 83: Comparison of CCN_0.3 and CCN_0.1 for entire study.

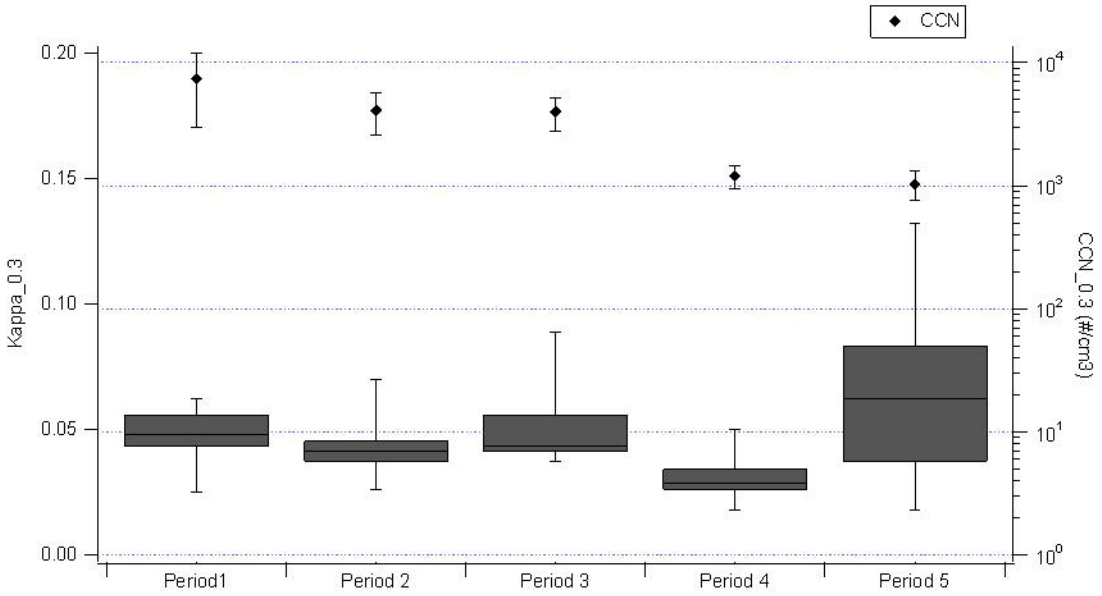

Figure 84: Single parameter hygroscopicity (Kappa) values of the particles during different air mass periods for CCN_0.3. The top of the boxes are the 3rd quartile of kappa values for that period, the bottoms are the 1st quartile values for that period. Whiskers show the minimum and maximum values for each period. Median values are the middle lines dividing the top and bottom of the boxes. Black diamonds are average CCN concentrations for those periods with standard deviation as error bars.

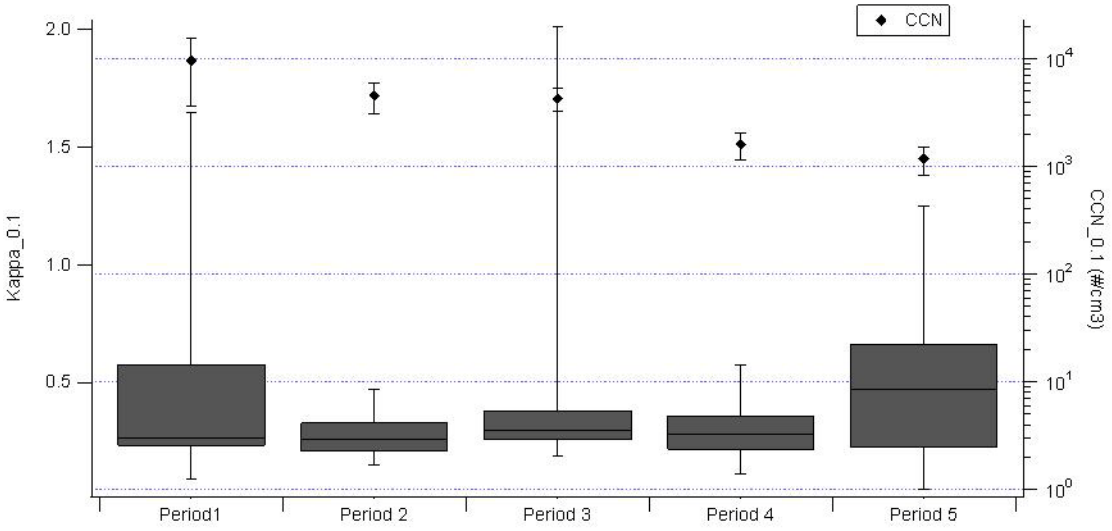

Figure 85: Single parameter hygroscopicity (Kappa) values of the particles during different air mass periods for CCN_0.1. The top of the boxes are the 3rd quartile of kappa values for that period, the bottoms are the 1st quartile values for that period. Whiskers show the minimum and maximum values for each period. Median values are the middle lines dividing the top and bottom of the boxes. Black diamonds are average CCN concentrations for those periods with standard deviation as error bars.

c. Air Mass and hygroscopicity

Shown in **Figure 82** and **Figure 83** are the κ values for the various air masses sampled during the fires, derived from CCN_0.3 with corresponding average CCN concentrations for each time period. The Santa Ana fire period's CCN activity was fairly constant with a κ range 0.015 - 0.07, with a median value of 0.045, close to κ of fresh anthropogenic emissions (0.05) when compared to previous studies (391). (391) measured the effect of atmospheric aging on the CCN activity of atmospheric aerosols by comparing different air masses with different degrees of aging during a research cruise in November 2004 along the southern coast of California over the Pacific Ocean. The local stagnation period (period 2) had κ values from 0.019 - 0.16, with a median value of 0.045, close to fresh anthropogenic emissions (0.05). The 1st ammonium period (period 3) had κ ranging from 0.019 - 0.15, with a median of 0.047, close to fresh anthropogenic emissions (0.05. Period 4 (2nd Ammonium period) κ ranged from 0.016 to 0.18, with a median of 0.041, close to fresh anthropogenic emissions (0.05). During period 5 (local ocean) the κ values had the widest range, from 0.004 to 0.3, with a median value of 0.052, where the air was stagnant and had mixing from various sources. Periods 1 -3 were the most dominated by BBA. The range of κ values during these periods was 0.015 – 0.16 with a median around 0.045. During a biomass influenced period in China (398) a κ value of 0.2 was measured, that of levoglucosan. Previous measurements of BBA hygroscopicity show a range of κ starting from 0.01 for fresh soot-rich biomass (358), 0.06 for ponderosa pine (370) up to a of κ of 0.55 for grass burning (358) and 0.7 for swamp sawgrass (370). (358) have noted aged biomass κ ranging from 0.1 to 0.3. (381) have observed a κ of 0.064 for filter of burned duff core extracted in methanol and 0.252

of burned sagebrush extracted in water. Therefore, it appears that the BBA in San Diego during October 2007 were somewhat below the range of previously determined biomass hygroscopicities, and likely had a large fraction of weakly hygroscopic and/or insoluble compounds present, producing the lower κ range observed. The large variability during the local ocean period (period 5) is most likely due to local meteorological events that were not captured during the HYSPLIT back trajectories, such as local sources. It is also important to note that κ values during the Santa Ana fire and local stagnation periods are just as CCN active as the κ values measured during the local ocean period, which is well after the fires that represents more typical background conditions in the San Diego area (**Figure 80** and **Figure 81**). While there could be influence from very local sources, these show that the BBA are moderately CCN active and as hygroscopic as ocean influenced periods, as shown in period 5. In addition, during period 5 CCN concentrations were 600-1200 cm^{-3} and particle counts were 3,000-23,000 cm^{-3}, those of a more typical San Diego background. However, as the wind started to shift from inland to from the coast/ocean, there was also a decrease in the fraction of biomass particles < 300nm, and an increase in elemental carbon particles (**Figure 81**).

iv. Conclusions

During the San Diego Wildfires 2007, aerosol size, composition and hygroscopicity were measured in real-time. With the decreased contribution of flaming fires, both Urey Hall CCN_0.3 concentrations and fCCN_0.3 decreased overtime, indicating the dominant contribution of inorganic compounds to the CCN activity and particle hygroscopicity. As CCN concentrations and fCCN decreased overtime, total particle concentrations and the average particle size were both decreasing. The decrease in particle concentrations was caused by a decrease in the contribution of biomass particle counts. In addition, the decrease in contribution of inorganic compounds to the BBA could explain the decrease in CCN concentrations as the wildfires died out and the BBA became less dominant and more aged. Elemental carbon (EC) particles then became more dominant as the relative contribution of BBA decreased, but had no notable temporal variations, and did not correspond to changes in fraction of active particles or the CCN concentration. Therefore the changes in CCN activity and hygroscopicity can be contributed to BBA chemistry changes (aging, change from flaming to smoldering phase); and not to overall aerosol chemistry changes with the influx of EC particles' increasing contribution to total aerosol fraction < 300nm during the duration of this study.

The lower κ range observed in this study for Urey Hall CCN (0.004 – 0.3) indicates that there were non-hygroscopic or insoluble compounds also present in the biomass burning aerosol. Previous studies have indicated that soot rich biomass has a κ value of 0.01 (358); therefore biomass emissions in San Diego during the October 2007 Wildfires were generally lower than previously determined biomass burning hygroscopicities (0.06 - 0.7)(370).

BBA are important contributions to global CCN concentrations because they are significantly large in initial size for combustion particles, and hygroscopic enough to activate into cloud droplets under typical supersaturations. Changes in the BBA chemistry and a dominating contribution of BBA to total particles, as we have shown here, can have a large effect on CCN concentration and particle hygroscopicity.

v. Acknowledgements

The authors are grateful to Andy Ault, Cassandra Gaston, and Melanie Zauscher for their help with data collection. They are also grateful to Dr. Satoshi Takahama (UCSD) for his helpful discussions and assistance with data analysis. Funding was provided by the California Air Resources Board grant # 04-336.